Diffusion Tensor Imaging in Idiopathic REM Sleep Behavior Disorder Reveals Microstructural Changes in the Brainstem, Substantia Nigra, Olfactory Region, and Other Brain Regions

Marcus M. Unger, MD[a1]; Marcus Belke[a1]; Katja Menzler, MD[1]; Johannes T. Heverhagen, MD, PhD[2]; Boris Keil[2]; Karin Stiasny-Kolster, MD[1]; Felix Rosenow, MD[1]; Nico J. Diederich, MD[3]; Geert Mayer, MD[4]; Jens C. Möller, MD[1]; Wolfgang H. Oertel, MD[a1]; Susanne Knake, MD[a1]

[a]All authors noted contributed equally to this work.

[1]Department of Neurology and [2]Department of Diagnostic Radiology, Philipps-Universität Marburg, Marburg, Germany; [3]Department of Neurosciences, Centre Hospitalier de Luxembourg, Luxembourg; [4]Hephata-Clinic for Neurology, Schwalmstadt-Treysa, Germany

Study Objectives: Idiopathic rapid eye movement sleep behavior disorder (iRBD)—a parasomnia characterized by dream enactments—is a risk marker for the development of Parkinson disease (PD) and other α-synucleinopathies. The pathophysiology of iRBD is likely due to dysfunction of brainstem nuclei that regulate REM sleep. Diffusion tensor imaging (DTI) is a method for studying microstructural brain tissue integrity in vivo. We investigated whether DTI detects microstructural abnormalities in the brain of patients with iRBD—compared with age-matched control subjects—as an in vivo potential indicator for changes related to "preclinical (premotor)" neuropathology in PD.

Design: N/A

Patients: Patients with iRBD (n = 12) and age-matched healthy control subjects (n = 12) were studied.

Interventions: At a 1.5T MRI maschine, whole-head DTI scans of fractional anisotropy, axial diffusivity (a potential marker of neuronal loss), and radial diffusivity (a potential marker of glial pathology) were analyzed using track-based spatial statistics, and 2 types of group analysis tools (FreeSurfer and FSL).

Measurements and Results: We found significant microstructural changes in the white matter of the brainstem ($P < 0.0001$), the right substantia nigra, the olfactory region, the left temporal lobe, the fornix, the internal capsule, the corona radiata, and the right visual stream of the patients with iRBD.

Conclusions: Changes were identified in regions known to be involved in REM-sleep regulation and/or to exhibit neurodegenerative pathology in iRBD and/or early PD. The study findings suggest that iRBD-related microstructural abnormalities can be detected in vivo with DTI, a widely available MRI technique.

Keywords: RBD, MRI, Parkinson's disease, TBSS, DTI, Radial diffusivity

Citation: Unger MM; Belke M; Menzler K; Heverhagen JT; Keil B; Stiasny-Kolster K; Rosenow F; Diederich NJ; Mayer G; Möller JC; Oertel WH; Knake S. Diffusion tensor imaging in idiopathic REM sleep behavior disorder reveals microstructural changes in the brainstem, substantia nigra, olfactory region, and other brain regions. *SLEEP* 2010;33(6):767-773.

RAPID EYE MOVEMENT (REM) SLEEP BEHAVIOR DISORDER (RBD) IS A REM-PARASOMNIA THAT CLINICALLY PRESENTS WITH NOCTURNAL SPEECH AND motor activity reflecting the dream content of the patient during REM sleep.[1,2] Idiopathic RBD (iRBD), i.e., the occurrence of RBD in the absence of other medical (neurologic) conditions, is considered to represent a clinical risk marker, with the—at present—highest positive predictive value for the subsequent development of an α-synucleinopathy, i.e., for Parkinson disease (PD), dementia with Lewy bodies, or multiple system atrophy.[3] In the context of evolving PD, iRBD is thought to be an early clinical correlate of a slowly progressing neurodegenerative process in the brainstem. Identification of such a neurodegenerative process with a routinely available technique such as magnetic resonance imaging (MRI) could be of value for the preclinical (premotor) detection of PD and other α-synucleinopathies.

During physiologic REM sleep, the activity of spinal α-motor neurons is suppressed by a complex interaction of superordinate brainstem nuclei (REM-on and REM-off areas, including the sublaterodorsal nucleus[4]). In RBD, this interaction between REM-on and REM-off areas is considered to be disturbed, leading to a disinhibition of spinal α-motor neurons and, subsequently, to movements during the dream phase. The sublaterodorsal nucleus is presumably one major efferent pathway for mediating muscle atonia during REM sleep,[5] pointing to the brainstem as a potential area to be investigated for structural changes in iRBD.

Until now, structural brain changes have not been described in patients with iRBD. Functional imaging studies have reported normal or conflicting findings: a single-photon emission computed tomography (SPECT) study showed that decreased blood flow in the pons and in the superior frontal lobes of patients with iRBD,[6] whereas other studies have confirmed the decreased perfusion in the frontal cortices, they have also found an increased perfusion in the pons, putamina, and right hippocampus.[7] SPECT studies using ligands to visualize the presynaptic dopamine transporter have reported that tracer uptake in the striatum is frequently reduced in patients with iRBD.[8-11] The latter finding must be interpreted in the context of iRBD as a pu-

A commentary on this article appears in this issue on page 731.

Submitted for publication July, 2009
Submitted in final revised form February, 2010
Accepted for publication March, 2010

Address correspondence to: Susanne Knake, MD, Department of Neurology, Philipps-University Marburg, Rudolf-Bultmann-Strasse 8, 35033 Marburg, Germany; Tel: 49 6421 58 65200; Fax: 49 6421 58 65208; E-mail: knake@staff.uni-marburg.de

tative "preclinical (premotor)" stage of the α-synucleinopathy PD, rather than as a finding that directly relates to the disruptive nocturnal behavior of RBD-related pathophysiology. The results of previous magnetic resonance spectroscopy studies are conflicting, reporting either no metabolic changes[12] or a pathologic choline/creatine ratio in the brainstem.[13] Recently, transcranial sonography has revealed hyperechogenicity in the substantia nigra in a group of patients with iRBD,[11,14] a sonographic marker that is seen in 90% of all patients with PD. In summary, in vivo imaging studies have not consistently demonstrated disease-specific structural abnormalities in patients with iRBD.

Diffusion tensor imaging (DTI) is a novel MRI technique that enables noninvasive in vivo visualization of brain white-matter microstructure. DTI has been applied successfully to several neurodegenerative disorders, providing insights into the pathophysiology of the respective disorders.[15-18] Most DTI studies have focused on fractional anisotropy (FA) as an unspecific summary measure of brain-tissue integrity. More recently, 2 components of the diffusion signal, namely axial diffusivity (AD) and radial diffusivity (RD), have been used to describe different aspects of mechanisms of degeneration. In the current study, the microstructural properties of the brains of patients with iRBD and age-matched healthy volunteers were examined using an automated whole-head analysis of the DTI measures of FA, RD, and AD.

METHODS

The study protocol was reviewed and approved by the local institutional review board. All enrolled subjects provided written informed consent to participate in this study.

Subjects

Twelve patients with iRBD and 12 healthy age-matched volunteers were included in the study. All enrolled patients with iRBD had a videopolysomnographically confirmed diagnosis of iRBD according to the revised version of the *International Classification of Sleep Disorders*.[19] Control subjects had no history of neurologic, psychiatric, or systemic illness and no family history of neurodegenerative disorders. All patients underwent a thorough neurologic examination, including Mini-Mental State Examination (MMSE) testing and a threshold-discrimination-identification olfactory function test with Sniffin' Sticks (Burghart Medizintechnik, Wedel, Germany). Control subjects were age matched, but not sex matched, because previous studies revealed age as being the most important variable influencing DTI results.[20]

MRI Acquisition

Microstructural brain-tissue integrity was assessed using DTI measures of FA and diffusivity (AD and RD[21-23]). The DTI scans were collected on a Siemens 1.5-T Sonata MRI scanner (Siemens Medical Solutions, Erlangen, Germany), using a circularly polarized head array coil. A single-shot echo planar sequence with a twice-refocused spin echo pulse, optimized to minimize eddy-current–induced image distortions,[24] was performed with the following parameters: TR/TE = 10600/104 ms, TI = -1 ms, flip angle = 90°, b = 1000 s/mm^2, 256 × 256 mm FOW, 128 × 128 × 60 matrix, and voxel size = 2 × 2 × 2.4 mm. Five T2 b0 images and 30 DWI b1000 images were collected during 1 scan. To minimize motion artifacts, the subjects' heads were firmly fixed in the head coil. All images were determined to be free of motion or ghosting or high-frequency or wrap-around artifacts at the time of image acquisition.

DTI Preprocessing and Analysis

Image preprocessing was performed as has been previously described[25]: diffusion volumes were motion corrected and averaged using FLIRT (FMRIB's Linear Image Registration Tool; http://www.fmrib.ox.ac.uk/analysis/research/flirt/)[26] with mutual information cost function to register each direction to the minimally eddy-current–distorted T2-weighted b0 DTI volume that had no diffusion weighting. Eigenvalues (λ_1, λ_2, λ_3) and eigenvectors of the diffusion tensor matrix for each voxel were computed from the DTI volumes for each subject on a voxel-by-voxel basis using conventional reconstruction methods.[27,28] The tools are included in the FreeSurfer package (FreeSurfer version 4.2.0; http://surfer.nmr.mgh.harvard.edu/).

FA and Diffusivity Map Calculation

The primary measure acquired from the DTI data was the FA, a scalar metric unit describing the white-matter microstructure. FA is dependent on the orientational coherence of the diffusion compartments within a voxel.[29] FA was calculated using the standard previously defined formula.[30] We additionally calculated measures of AD (λ_1) and RD ($[\lambda_2+\lambda_3]/2$).[21-23]

T2 b0 images were obtained using the same parameters as those used for the diffusion sensitive images except without any diffusion weighting. Those images were analyzed to determine whether changes other than those in tissue microstructure contributed to the observed effects, such as technical artifacts or individual large-scale signal changes such as white-matter signal abnormalities (e.g., hyperintensities).

Nonlinear Registration and Tract-based Spatial Statistics

Voxelwise statistical analysis of the FA data was carried out using tract-based spatial statistics (TBSS; tract-based spatial statistics[31]), which is part of the FSL data-analysis suite (FSL 4.1.2; http://www.fmrib.ox.ac.uk/fsl/).[32] First, the T2 b0 images were brain extracted using the BET-tool of the FSL stream. Those extracted brains were used to mask the FA images. All subjects' masked FA data were then aligned into a common space using the nonlinear registration tool FNIRT,[33] which uses a b-spline representation of the registration warp field.[34] The common space was given by the automatically selected subject that was most representative of the whole group. This subject was affinely registered to the T1 template in MNI 152 standard space. Next, a mean FA image was created and thinned to create a mean FA skeleton, which represents the centers of all tracts the group has in common. A threshold of FA greater than 0.2 was applied to the skeleton to include only major fiber bundles. Each subject's aligned FA data was then projected onto this skeleton. Data along the skeleton was smoothed utilizing an anatomic constraint to limit the smoothing to neighboring data within adjacent voxels along the skeleton. For smoothing, the neighboring voxels within a cube of 6-mm edge length were used to calculate the mean. The smoothing step was performed using Matlab (Matlab 7.6.0.324, MathWorks, Aachen, Germa-

ny). All analyses were masked to display regions only with FA values of greater than 0.2 as an additional procedure to avoid examination of regions that are likely comprised of multiple tissue types or fiber orientations. The exact transformations derived for the anisotropy maps were applied to the AD and RD volumes for matched processing of all image volumes.

Group Analysis

Two data-analysis approaches (FreeSurfer and FSL) were used for group analysis.

FreeSurfer approach

The resulting skeletonized images were fed into voxelwise cross-subject statistics. For the group analysis, we used the tool mri_glmfit of the FreeSurfer stream. The data was fit into a generalized linear model, and an unpaired t test was performed. The resulting data were corrected for multiple comparisons by a permutation-based approach.[35] Therefore, 12.000 simulations were performed under the null hypothesis; this approach was based on the AFNI null-z simulator (AlphaSim; http://afni.nimh.nih.gov/afni/doc/manual/AlphaSim). Last, the data were clustered; in this step, several connected voxels were searched and merged into 1 cluster. For the clustering, we considered only voxels with a minimum significance of $P < 0.01$. To display the results, all figures were made with the exact same parameters, showing clusters with a significance of $P < 0.01$; all regions were dilated for better visualization using the dilM function of the FSL tool fslmaths. (Figure 1) The correction for multiple testing was performed with the mri_glmfit-sim tool of the FreeSurfer package. Results were summarized in tables showing the localization of the clusters and their significances (Tables 2-4)

FSL standard approach

For comparison of identified regions, data were also analyzed using the established standard FSL approach for group statistics. The skeletonized images resulting from the TBSS procedure were processed using the randomize GLM tool of the FSL stream. For this procedure, we followed the standard instructions for performing a GLM test: First, a design matrix and a contrast matrix were created with the FSL-tool design_ttest2, then the tool randomize from the FSL stream was applied with the standard parameters for the TBSS-analysis. The correction for multiple testing was performed using the FSL tool randomize using the same parameters as for mri_glmfit-sim. Again, 12.000 permutations were performed, and, afterward, the results were clustered. To display the results, all figures were calculated with the exact same parameters as in FreeSurfer, showing voxels with a significance of $P < 0.01$. All regions were dilated for better visualization, using the dilM function of the FSL tool fslmaths.

RESULTS

The main demographic and clinical data of all enrolled subjects are summarized in Table 1. We investigated 12 patients with iRBD and 12 age-matched control subjects using whole-brain DTI. Accordingly, in the neurologic examination, none of the patients with iRBD fulfilled the UK Brain Bank Criteria for the diagnosis of PD.[36]

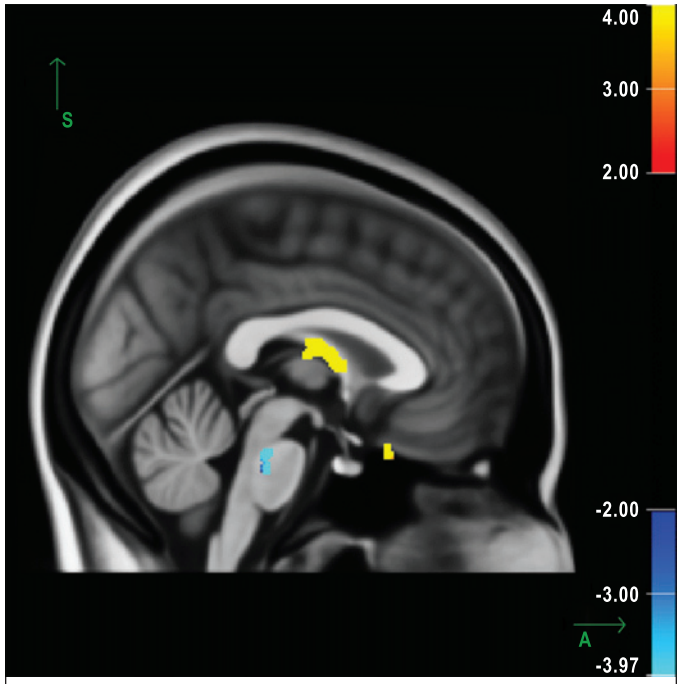

Figure 1—Sagittal view of the average b0 image, calculated from all study subjects (or representing the average of all subjects in the study), showing the white-matter skeleton all subjects have in common. Significant increases in radial diffusivity can be observed in the fornix and the olfactory region ($P < 0.0001$). A significant decrease in the axial diffusivity can be seen in the pons ($P < 0.0001$). Results are displayed as the negative decadic logarithm of the P value ($P = 10^{-x}$). The increase in radial diffusivity is shown in red-yellow; the decrease in axial diffusivity, in blue-light blue.

Table 1—Demographics and diagnostic findings among 12 subjects with iRBD and 12 control subjects

Demographics	Subjects with iRBD	Control subjects
Men	11	3
Age, y	59 ± 10.5 (38-71)	56.8 ± 10.6 (42-74)
Clinical scores		
MMSE	29.2 ± 0.8 (26-30)	NA
TDI sum score	23 ± 9.4 (8-35)	NA
Imaging study results		
FP-CIT SPECT tracer uptake[a]		
Normal	3	NA
Reduced or asymmetric	4	NA

Data are shown as mean + SD (range) or number. MMSE refers to Mini-Mental Status Examination; TDI, the threshold-discrimination-identification in the Sniffin' Stick Test (a TDI sum score ≥ 30 is defined as normosmia).[64]

[a]Data are from 7 subjects with idiopathic rapid eye movement sleep behavior disorder (iRBD) who agreed to undergo ^{123}I-N-Ω-fluoropropyl-2β-carbomethoxy-3β-(4-iodophenyl)-nortropane single photon emission tomography (FP-CIT SPECT) scanning.

FA Results

Significant FA increases (corrected $P < 0.0001$) were found in the internal capsule bilaterally (along the anterior thalamic radiation) and in the olfactory region, whereas significant

Table 2—Regions with significant changes in fractional anisotropy

Region	Size, mm³	Maximum log-transformed P, 10^-x	Corrected overall P value	X	Y	Z
Right visual stream	483	(-) 4.58	< 0. 0001	12	-93	12
Fornix	158	(-) 4.39	< 0. 0001	3	-9	13
Left superior temporal lobe	333	(-) 4.16	< 0. 0001	-60	-20	4
Olfactory region						
Right	38	2.11	< 0. 0001	8	32	-18
Left	73	2.4	< 0. 0001	-5	39	-23
Internal capsule						
Right	37	2.05	< 0. 0001	19	9	-8
Left	199	3.74	< 0. 0001	-15	13	-5

The results of the statistical tests were corrected for multiple testing, and regions with clusters of several connected voxels (with a minimum significance of P < 0.01) were searched. X, Y, and Z refer to the corresponding MNI-atlas coordinates.

Table 3—Regions with significant changes in axial diffusivity

Region	Size, mm³	Maximum log-transformed P, 10^-x	Corrected overall P value	X	Y	Z
Pons	425	3.37	< 0. 0001	2	-29	-30
Corona radiata						
Right	382	4.42	< 0. 0001	13	6	54
Left	153	2.89	< 0. 0001	-6	38	45
Substantia nigra	9	1.98	< 0. 0001	14	-17	-14

The results of the statistical tests were corrected for multiple testing, and regions with clusters of several connected voxels (with a minimum significance of P < 0.01) were searched. X, Y, and Z refer to the corresponding MNI-atlas coordinates.

Table 4—Regions with significant changes in radial diffusivity

Region	Size, mm³	Maximum log-transformed P, 10^-x	Corrected overall P value	X	Y	Z
Right visual stream	979	4.08	< 0. 0001	36	-79	-4
Fornix	165	2.86	< 0. 0001	4	-11	13
Left superior temporal lobe	103	2.58	< 0. 0001	-60	-18	3

The results of the statistical tests were corrected for multiple testing, and regions with clusters of several connected voxels (with a minimum significance of P < 0.01) were searched. X, Y, and Z refer to the corresponding MNI-atlas coordinates.

decreases were found in the fornix, the right visual stream (V1,V2), and the left superior temporal lobe. Figure 1, supplementary Figure S1 (supplementary figures are available online only at www.journalsleep.org), and Table 2 show the regions with the main changes in FA.

AD and RD Results

AD describes the principal eigenvector (λ1) and is assumed to contribute information regarding the integrity of axons[37] or changes in extraaxonal/extracellular space.[38] Regional reductions in AD seem to represent regions with altered axonal integrity.[37] Significant decreases (corrected P < 0.0001) in the axial diffusivity were observed in the brainstem, i.e., in the pons and the right substantia nigra. Changes also occurred in the corona radiata bilaterally. Changes in AD are shown in Figure 1, supplementary Figure S2, and Table 3.

RD describes an average of the eigenvectors perpendicular to the principal direction ([λ2 + λ3]/2).[22,23,39,40] Regional increases in RD are considered to be associated with changes in myelination or glial cell morphology.[22,23,40] In our study, patients with iRBD had significantly increased RD (corrected P < 0.0001) in the fornix, the right visual stream (V1,V2), and the left superior temporal lobe. as shown in supplementary Figure S3 and Table 4.

Comparison Between the 2 Data-Analysis Methods

Two approaches for data analysis were used for group comparisons: the tool Randomize of the FSL data analysis suite and the approach using the mri_glmfit of the FreeSurfer package identified the same pattern of microstructural tissue alteration, as shown in the supplementary Figure S4.

DISCUSSION

Until now, no structural abnormalities have been described in patients with iRBD using MRI or other structural imaging techniques. Here, we report focal microstructural brain changes in the white matter of the brain of patients with a videopolysomnographically confirmed diagnosis of iRBD using DTI with a hypothesis-free approach. DTI measures the diffusional motion of water molecules, which is predetermined by the (sub)cellular microenvironment. By this means, DTI can be used as a sensitive measure of microstructural integrity. The diffusion within a single voxel can be expressed as FA, a metric measure ranging from 0 (isotropic) to 1 (anisotropic). The FA is high (close to 1) in regions in which diffusion is restricted to 1 orientation, e.g., along highly organized structures, like bundles of myelinated fibers, whereas the FA is low (close to 0) in less-organized structures, such as regions of cellular damage in which diffusion tends to be equally likely in all directions (i.e., isotropic).

Localization of Microstructural Brain Changes

Alterations in microstructure were found in the iRBD group compared with control subjects in brainstem regions known to regulate REM sleep, as well as in the olfactory region, the thalamic radiation in the anterior limb of the internal capsule, the right substantia nigra, the left superior temporal lobe and the right occipital lobe, and the fornix.

We found a widespread decrease in AD (indicating possible axonal damage) in the brainstem, especially the pons, i.e., re-

gions known to be involved in the regulation of REM sleep.[4] Dysfunction of the respective structures is thought to be the pathophysiologic correlate of RBD.[5] This assumption is compatible with the results of postmortem studies that describe degeneration of monoaminergic neurons and the presence of Lewy bodies in brainstem structures in patients with RBD.[41,42] Furthermore, structural brainstem lesions that affect the sublaterodorsal nucleus (its afferent or efferent pathways and linked nuclei, respectively) have been shown to result in symptomatic RBD.[43-46] Finally, experimental lesions in the ventral part of the pons and the ventral mesopontine junction in animal models can provoke an RBD-like phenotype as well.[47] The reported morphologic in vivo changes seen in the brainstem of our iRBD population overlap with anatomic regions that are thought to be responsible for mediating muscle atonia during REM sleep.

According to the Braak pathoanatomic model of PD (which is based on a cross-sectional cliniconeuropathologic study),[48-50] the olfactory bulb, as well as the medulla oblongata and the pons, exhibit Lewy body pathology prior to the occurrence of Lewy body pathology in mesencephalic neurons in the substantia nigra. Braak staging is not undisputed,[51] which is in part due to the fact that Lewy body pathology can also occur in the absence of any neurologic signs. Therefore, Lewy body pathology in the lower brainstem might not unavoidably constitute a preclinical stage of PD. Nevertheless, Braak staging is likely to represent an approximate model for the development of sporadic PD in a large number of cases. The Braak hypothesis is compatible with retrospective clinical and neuropathologic studies[12,42] that show that iRBD can represent a premotor stage of an underlying α-synucleinopathy.

Patients with iRBD also frequently show hyposmia,[10,52] a fact that is also compatible with the concept of iRBD as a premotor manifestation of PD. In accordance with this clinical symptom, we found a bilateral increase in global FA and a decrease in RD in the olfactory region of patients with iRBD, suggestive of disturbed microstructure and demyelination in this area.[22,23,40] Previous DTI studies in patients with PD have not detected abnormalities in the olfactory region. This might be due to methodologic aspects: brain regions adjacent to cerebrospinal fluid (like the olfactory region) are prone to artifacts and registration errors, especially when using linear registration tools. We tried to minimize those artifacts by using the novel technique of TBSS and a nonlinear registration[31] (for olfactory bulb, see discussion of methodologic aspects).

Changes in AD were seen also in the right substantia nigra. This finding supports the concept of iRBD as a preclinical stage of PD and is in line with 2 recently published studies reporting comparable FA changes in regions of interest in the substantia nigra of patients with PD.[15,18] The fact that we observed significant changes in the substantia nigra on only 1 side might reflect the typical asymmetric onset of PD and the potential transition state from iRBD to PD in some of our patients.

Another brain region exhibiting structural differences (FA changes and changes in RD) between iRBD patients and control subjects in our study is the fornix. FA changes in the fornix have already been described for patients with PD and are thought to be involved in the generation of excessive daytime sleepiness.[53] This may be of relevance because excessive daytime sleepiness has also been described in the preclinical phase of PD.[54] Furthermore, the results of experimental studies have suggested that the perifornical region is involved in the regulation of REM sleep.[55,56] Impaired color discrimination has been described clinically in drug-naïve patients with early-stage PD[57] as well as in patients with iRBD.[58] Consequently, impaired color discrimination is thought to be an early clinical feature of the disorders that deteriorates over time[59] as the neurodegenerative process progresses. Impaired color discrimination in patients with iRBD and PD has been explained by degeneration of retinal neurons, yet there is still a lack of clear evidence concerning the structural neuropathologic correlate of this clinical sign. Our finding of FA changes and changes in RD in the right visual stream (V2 area) raise the question of whether the anatomic correlate for impaired color discrimination might be additionally located in the visual pathway.

We found microstructural changes in the left anterior thalamic radiation and in the left temporal lobe, which may account for neuropsychological deficits in patients with iRBD. Indeed, disruption of the left anterior thalamic radiation has been shown to result in memory dysfunction[60]; in addition, the left temporal lobe is involved in memory and verbal processing. The fact that some of our findings were seen only unilaterally might reflect the asymmetry of the neurodegenerative process in PD. However, the clinical impact of these findings remains speculative and needs further validation.

Discussion of Methodologic Aspects

Our study was performed without any a-priori hypothesis (i.e., predefined regions of interest). We used the method of nonlinear registration (TBSS) to control for method-inherent shortcomings of DTI, such as registration and spatial smoothing errors. For technical reasons, we did not find changes in small brain regions like the olfactory bulb. Due to its size and location, the olfactory bulb is prone to susceptibility artifacts, and the large degree of interindividual anatomy in the olfactory bulb will lead to coregistration problems. Using TBSS, the olfactory bulb will not be displayed because only brain tissue with low intraindividual anatomic variability is included.

Two different approaches were used for statistical-group comparisons. Both techniques, FSL and FreeSurfer, identified the same pattern of microstructural tissue alteration, supporting the goal of the FSL and the FreeSurfer teams to make interoperation of FSL and FreeSurfer as easy as possible.

DTI is a technique that can quantify alterations in tissue microstructure regardless of the underlying pathologic mechanisms. FA) is the most commonly used parameter in DTI studies. FA is an unspecific measure of white-matter integrity. Recently, studies have focused on the calculation of RD and AD. Changes in these values might be more specific: previous work in animal models described a correlation between axonal loss and a decrease in AD as well as a correlation between an increase in RD and demyelination.[22,23,61,62,63] Recently, using combined radiologic and neuropathologic assessment of unfixed brain tissue that was collected post-mortem, these hypotheses were confirmed in humans with multiple sclerosis.[63] Nevertheless, detailed histopathologic validation in healthy humans is still missing.[22,23,63]

DTI is still a nonspecific measure that does not provide information about the underlying causes for the reported microstruc-

tural pathology. Nevertheless, our study hints at new potential neuropathologic correlates of iRBD that need to be further validated in postmortem studies. Likewise, future research is necessary to determine the sensitivity and specificity of this technique as a potential early marker for a neurodegenerative process in iRBD as a predictor for α-synucleinopathies, such as PD. In addition, long-term studies are needed to address the question of whether the identified pathologic signals in FA, AD and RD, change over time and whether these signals might be useful to monitor disease progression.

CONCLUSION

In conclusion, our DTI study describes in vivo specific microanatomic alterations in the brain of patients with the so-called idiopathic form of RBD. Our findings are compatible with the current hypotheses about the location of RBD pathology and its association with PD. The observed changes in the pons are perhaps representative of a structural correlate for the disruptive, dream-enacting behavior during REM sleep. Changes seen in the substantia nigra are in accordance with the assumption that iRBD may represent a preclinical (premotor) stage of PD. Our study suggests that RBD-related neuropathology can be detected in vivo with a widely available MRI technology.

ACKNOWLEDGMENTS

This work was supported by the Willy Robert Pitzer Foundation (to SK and WHO), the Förderverein Neurologie Marburg (to SK), and the BMBF (to WHO, funding code: 01GI0401) and partly supported by a UKGM Research Grant (to SK and WHO). We thank all patients and healthy control subjects who participated in this study.

DISCLOSURE STATEMENT

This was not an industry supported study. Dr. Stiasny-Kolster has been on the advisory boards of Boehringer Ingelheim, Orion, Mundipharmi, and Schwarz Pharma and has participated in speaking engagements for Schwarz Pharma, UCB, Boehringer Ingelheim, and Hoffmann-LaRoche. Dr. Rosenow has received research support from UCB and has been on the advisory boards of UCB, Pfizer, and GlaxoSmithKline. Dr. Mayer has participated in speaking engagaments for UCB, Sanofi-Aventis, GlaxoSmithKline, and Cephalon. Dr. Oertel has received research support from Novartis; has participated in speaking engagements for Desitin, Boehrunger Engelheim, GlaxoSmithKline, TEVA, Orion Pharma, Novartis, Schwarz Pharma, and Neuroscience; and has consulted for Novartis, Orion Pharma, Neuroscience, Solvay Pharmaceuticals International, Desitin, Boehringer Ingelheim, GlaxoSmithKline, Teva, Protosys, and Sysnosia.

REFERENCES

1. Schenck CH, Bundlie SR, Ettinger MG, Mahowald MW. Chronic behavioral disorders of human REM sleep: a new category of parasomnia. Sleep 1986;9:293-308.
2. Schenck CH, Bundlie SR, Patterson AL, Mahowald MW. Rapid eye movement sleep behavior disorder. A treatable parasomnia affecting older adults. JAMA 1987;257:1786-9.
3. Iranzo A, Molinuevo JL, Santamaria J, et al. Rapid-eye-movement sleep behaviour disorder as an early marker for a neurodegenerative disorder: a descriptive study. Lancet Neurol 2006;5:572-7.
4. Lu J, Sherman D, Devor M, Saper CB. A putative flip-flop switch for control of REM sleep. Nature 2006;441:589-94.
5. Boeve BF, Silber MH, Saper CB, et al. Pathophysiology of REM sleep behaviour disorder and relevance to neurodegenerative disease. Brain 2007;130:2770-88.
6. Shirakawa S, Takeuchi N, Uchimura N, et al. Study of image findings in rapid eye movement sleep behavioural disorder. Psychiatry Clin Neurosci 2002;56:291-2.
7. Mazza S, Soucy JP, Gravel P, et al. Assessing whole brain perfusion changes in patients with REM sleep behavior disorder. Neurology 2006;67:1618-22.
8. Eisensehr I, Linke R, Noachtar S, Schwarz J, Gildehaus FJ, Tatsch K. Reduced striatal dopamine transporters in idiopathic rapid eye movement sleep behaviour disorder. Comparison with Parkinson's disease and controls. Brain 2000;123:1155-60.
9. Eisensehr I, Linke R, Tatsch K, et al. Increased muscle activity during rapid eye movement sleep correlates with decrease of striatal presynaptic dopamine transporters. IPT and IBZM SPECT imaging in subclinical and clinically manifest idiopathic REM sleep behavior disorder, Parkinson's disease, and controls. Sleep 2003;26:507-12.
10. Stiasny-Kolster K, Doerr Y, Moller JC, et al. Combination of 'idiopathic' REM sleep behaviour disorder and olfactory dysfunction as possible indicator for alpha-synucleinopathy demonstrated by dopamine transporter FP-CIT-SPECT. Brain 2005;128:126-37.
11. Unger MM, Moller JC, Stiasny-Kolster K, et al. Assessment of idiopathic rapid-eye-movement sleep behavior disorder by transcranial sonography, olfactory function test, and FP-CIT-SPECT. Mov Disord 2008;23:596-9.
12. Iranzo A, Santamaria J, Pujol J, Moreno A, Deus J, Tolosa E. Brainstem proton magnetic resonance spectroscopy in idiopathic REM sleep behavior disorder. Sleep 2002;25:867-70.
13. Miyamoto M, Miyamoto T, Kubo J, Yokota N, Hirata K, Sato T. Brainstem function in rapid eye movement sleep behavior disorder: the evaluation of brainstem function by proton MR spectroscopy (1H-MRS). Psychiatry Clin Neurosci 2000;54:350-1.
14. Stockner H, Iranzo A, Seppi K, et al. Midbrain hyperechogenicity in idiopathic REM sleep behavior disorder. Mov Disord 2009;24:1906-9.
15. Gattellaro G, Minati L, Grisoli M, et al. White matter involvement in idiopathic Parkinson disease: a diffusion tensor imaging study. Am J Neuroradiol 2009;30:1222-6.
16. Knake S, Salat DH, Halgren E, Halko MA, Greve DN, Grant PE. Changes in white matter microstructure in patients with TLE and hippocampal sclerosis. Epileptic Disord 2009;11:244-50.
17. Rosas HD, Tuch DS, Hevelone ND, et al. Diffusion tensor imaging in presymptomatic and early Huntington's disease: selective white matter pathology and its relationship to clinical measures. Mov Disord 2006;21:1317-25.
18. Vaillancourt DE, Spraker MB, Prodoehl J, et al. High-resolution diffusion tensor imaging in the substantia nigra of de novo Parkinson disease. Neurology 2009;72:1378-84.
19. The International Classification of Sleep Disorders, revised: Diagnostic and Coding Manual. Westchester, IL: American Academy of Sleep Medicine; 2005.
20. Fjell AM, Westlye LT, Greve DN, et al. The relationship between diffusion tensor imaging and volumetry as measures of white matter properties. Neuroimage 2008;42:1654-68.
21. Budde MD, Kim JH, Liang HF, et al. Toward accurate diagnosis of white matter pathology using diffusion tensor imaging. Magn Reson Med 2007;57:688-95.
22. Song SK, Sun SW, Ju WK, Lin SJ, Cross AH, Neufeld AH. Diffusion tensor imaging detects and differentiates axon and myelin degeneration in mouse optic nerve after retinal ischemia. Neuroimage 2003;20:1714-22.
23. Song SK, Sun SW, Ramsbottom MJ, Chang C, Russell J, Cross AH. Dysmyelination revealed through MRI as increased radial (but unchanged axial) diffusion of water. Neuroimage 2002;17:1429-36.
24. Reese TG, Heid O, Weisskoff RM, Wedeen VJ. Reduction of eddy-current–induced distortion in diffusion MRI using a twice-refocused spin echo. Magn Reson Med 2003;49:177-82.
25. Salat DH, Tuch DS, Greve DN, et al. Age-related alterations in white matter microstructure measured by diffusion tensor imaging. Neurobiol Aging 2005;26:1215-27.
26. Jenkinson M, Bannister P, Brady M, Smith S. Improved optimization for the robust and accurate linear registration and motion correction of brain images. Neuroimage 2002;17:825-41.

27. Basser PJ, Mattiello J, LeBihan D. Estimation of the effective self-diffusion tensor from the NMR spin echo. J Magn Reson B 1994;103:247-54.
28. Basser PJ, Pierpaoli C. Microstructural and physiological features of tissues elucidated by quantitative-diffusion-tensor MRI. J Magn Reson B 1996;111:209-19.
29. Pierpaoli C, Basser PJ. Toward a quantitative assessment of diffusion anisotropy. Magn Reson Med 1996;36:893-906.
30. Basser PJ. New histological and physiological stains derived from diffusion-tensor MR images. Ann N Y Acad Sci 1997;820:123-38.
31. Smith SM, Jenkinson M, Johansen-Berg H, et al. Tract-based spatial statistics: voxelwise analysis of multi-subject diffusion data. Neuroimage 2006;31:1487-505.
32. Smith SM, Jenkinson M, Woolrich MW, et al. Advances in functional and structural MR image analysis and implementation as FSL. Neuroimage 2004;23:S208-19.
33. Andersson JLR JMaSS. Non-linear registration, aka Spatial normalisation. FMRIB technical report TR07JA2 from wwwfmriboxacuk/analysis/techrep; 2007.
34. Rueckert D, Sonoda LI, Hayes C, Hill DL, Leach MO, Hawkes DJ. Non-rigid registration using free-form deformations: application to breast MR images. IEEE Trans Med Imaging 1999;18:712-21.
35. Nichols TE, Holmes AP. Nonparametric permutation tests for functional neuroimaging: a primer with examples. Hum Brain Mapp 2002;15:1-25.
36. Gibb WR, Lees AJ. The relevance of the Lewy body to the pathogenesis of idiopathic Parkinson's disease. J Neurol Neurosurg Psychiatry 1988;51:745-52.
37. Glenn OA, Henry RG, Berman JI, et al. DTI-based three-dimensional tractography detects differences in the pyramidal tracts of infants and children with congenital hemiparesis. J Magn Reson Imaging 2003;18:641-8.
38. Beaulieu C, Allen PS. Determinants of anisotropic water diffusion in nerves. Magn Reson Med 1994;31:394-400.
39. Davis SW, Dennis NA, Buchler NG, White LE, Madden DJ, Cabeza R. Assessing the effects of age on long white matter tracts using diffusion tensor tractography. Neuroimage 2009;46:530-41.
40. Song SK, Yoshino J, Le TQ, et al. Demyelination increases radial diffusivity in corpus callosum of mouse brain. Neuroimage 2005;26:132-40.
41. Arnulf I, Bonnet AM, Damier P, et al. Hallucinations, REM sleep, and Parkinson's disease: a medical hypothesis. Neurology 2000;55:281-8.
42. Uchiyama M, Isse K, Tanaka K, et al. Incidental Lewy body disease in a patient with REM sleep behavior disorder. Neurology 1995;45:709-12.
43. Culebras A, Moore JT. Magnetic resonance findings in REM sleep behavior disorder. Neurology 1989;39:1519-23.
44. Kimura K, Tachibana N, Kohyama J, Otsuka Y, Fukazawa S, Waki R. A discrete pontine ischemic lesion could cause REM sleep behavior disorder. Neurology 2000;55:894-5.
45. Tippmann-Peikert M, Boeve BF, Keegan BM. REM sleep behavior disorder initiated by acute brainstem multiple sclerosis. Neurology 2006;66:1277-9.
46. Xi Z, Luning W. REM sleep behavior disorder in a patient with pontine stroke. Sleep Med 2009;10:143-6.
47. Lai YY, Hsieh KC, Nguyen D, Peever J, Siegel JM. Neurotoxic lesions at the ventral mesopontine junction change sleep time and muscle activity during sleep: an animal model of motor disorders in sleep. Neuroscience 2008;154:431-43.
48. Braak H, Del Tredici K, Bratzke H, Hamm-Clement J, Sandmann-Keil D, Rub U. Staging of the intracerebral inclusion body pathology associated with idiopathic Parkinson's disease (preclinical and clinical stages). J Neurol 2002;249Suppl 3:III/1-5.
49. Braak H, Del Tredici K, Rub U, de Vos RA, Jansen Steur EN, Braak E. Staging of brain pathology related to sporadic Parkinson's disease. Neurobiol Aging 2003;24:197-211.
50. Braak H, Ghebremedhin E, Rub U, Bratzke H, Del Tredici K. Stages in the development of Parkinson's disease-related pathology. Cell Tissue Res 2004;318:121-34.
51. Burke RE, Dauer WT, Vonsattel JP. A critical evaluation of the Braak staging scheme for Parkinson's disease. Ann Neurol 2008;64:485-91.
52. Fantini ML, Postuma RB, Montplaisir J, Ferini-Strambi L. Olfactory deficit in idiopathic rapid eye movements sleep behavior disorder. Brain Res Bull 2006;70:386-90.
53. Matsui H, Nishinaka K, Oda M, et al. Disruptions of the fornix fiber in Parkinsonian patients with excessive daytime sleepiness. Parkinsonism Relat Disord 2006;12:319-22.
54. Abbott RD, Ross GW, White LR, et al. Excessive daytime sleepiness and subsequent development of Parkinson disease. Neurology.2005;65:1442-6.
55. Koyama Y, Takahashi K, Kodama T, Kayama Y. State-dependent activity of neurons in the perifornical hypothalamic area during sleep and waking. Neuroscience 2003;119:1209-19.
56. Lu JW, Fenik VB, Branconi JL, Mann GL, Rukhadze I, Kubin L. Disinhibition of perifornical hypothalamic neurones activates noradrenergic neurones and blocks pontine carbachol-induced REM sleep-like episodes in rats. J Physiol 2007;582:553-67.
57. Buttner T, Kuhn W, Muller T, Patzold T, Heidbrink K, Przuntek H. Distorted color discrimination in 'de novo' parkinsonian patients. Neurology 1995;45:386-7.
58. Postuma RB, Lang AE, Massicotte-Marquez J, Montplaisir J. Potential early markers of Parkinson disease in idiopathic REM sleep behavior disorder. Neurology 2006;66:845-51.
59. Diederich NJ, Raman R, Leurgans S, Goetz CG. Progressive worsening of spatial and chromatic processing deficits in Parkinson disease. Arch Neurol 2002;59:1249-52.
60. Stenset V, Grambaite R, Reinvang I, et al. Diaschisis after thalamic stroke: a comparison of metabolic and structural changes in a patient with amnesic syndrome. Acta Neurol Scand Suppl 2007;187:68-71.
61. Kim JH, Loy DN, Liang HF, Trinkaus K, Schmidt RE, Song SK. Noninvasive diffusion tensor imaging of evolving white matter pathology in a mouse model of acute spinal cord injury. Magn Reson Med 2007;58:253-60.
62. Sun SW, Liang HF, Le TQ, Armstrong RC, Cross AH, Song SK. Differential sensitivity of in vivo and ex vivo diffusion tensor imaging to evolving optic nerve injury in mice with retinal ischemia. Neuroimage 2006;32:1195-204.
63. Schmierer K, Wheeler-Kingshott CA, Boulby PA, et al. Diffusion tensor imaging of post mortem multiple sclerosis brain. Neuroimage 2007;35:467-77.
64. Kobal G, Klimek L, Wolfensberger M, et al. Multicenter investigation of 1,036 subjects using a standardized method for the assessment of olfactory function combining tests of odor identification, odor discrimination, and olfactory thresholds. Eur Arch Otorhinolaryngol 2000;257:205-11.

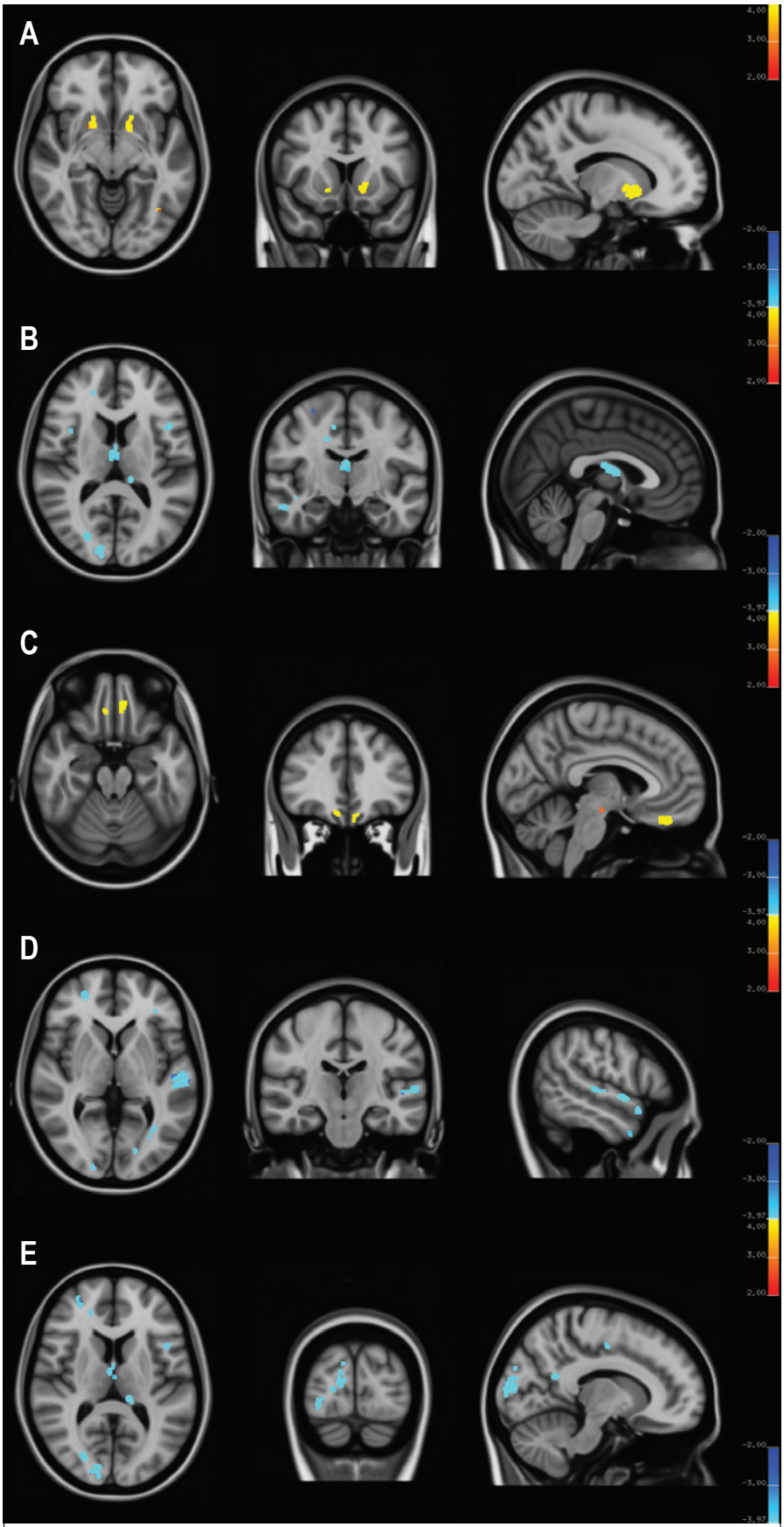

Figure S1—Regions with significant changes in fractional anisotropy, displayed as the negative decadic logarithm of the P value ($P = 10^{-x}$). Panel A, internal capsule; panel B, fornix; panel C, olfactory cortex; panel D, left temporal cortex; panel E, right visual cortex. Increases in fractional anisotropy are shown in red-yellow; decreases in blue-green.

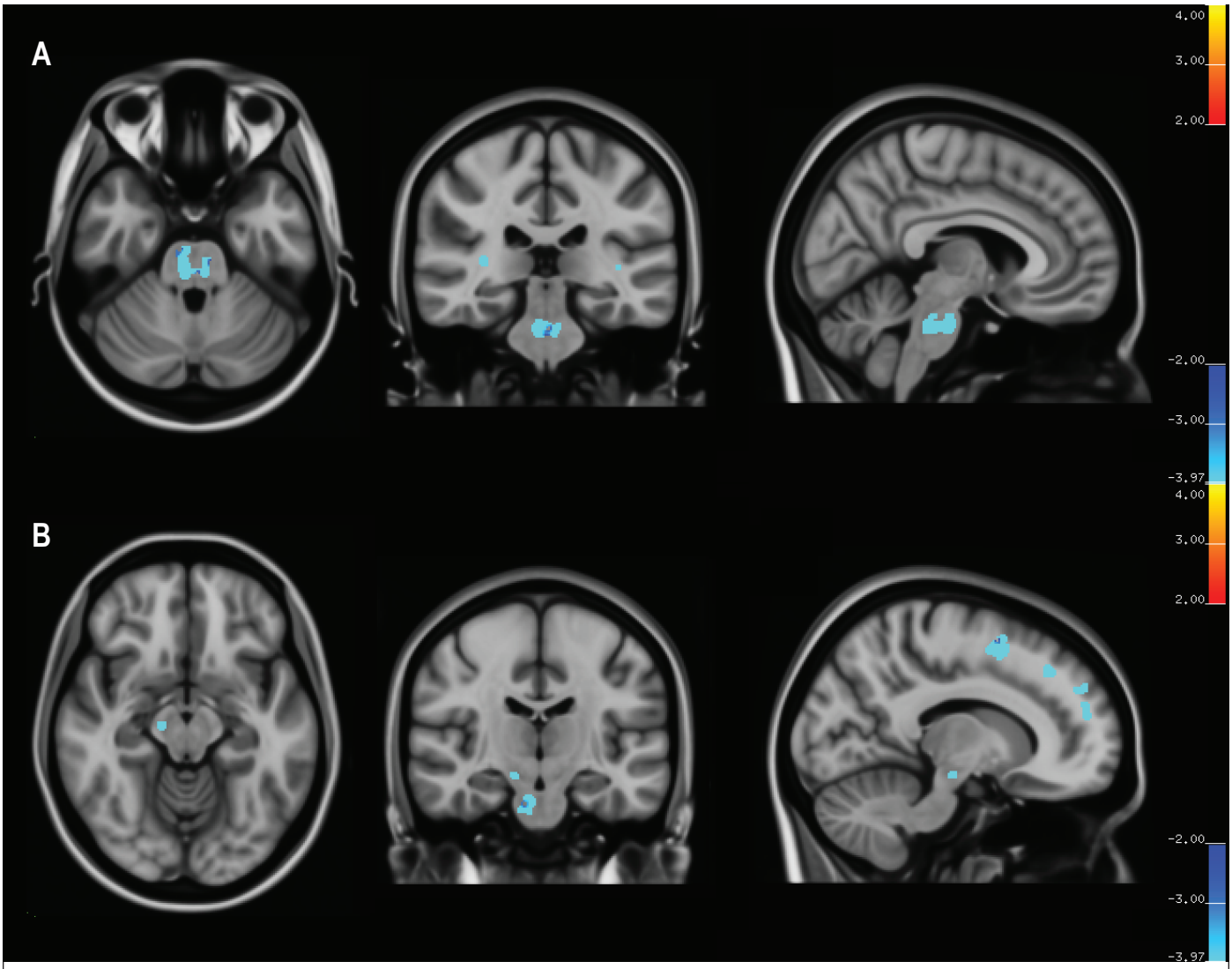

Figure S2—Regions with significant changes in axial diffusivity, a potential measure of axonal damage. Significant changes are displayed as the negative decadic logarithm of the P value ($P = 10^{-x}$). Panel A, pons; panel B, right substantia nigra. Decreases in axial diffusivity are shown in blue-green.

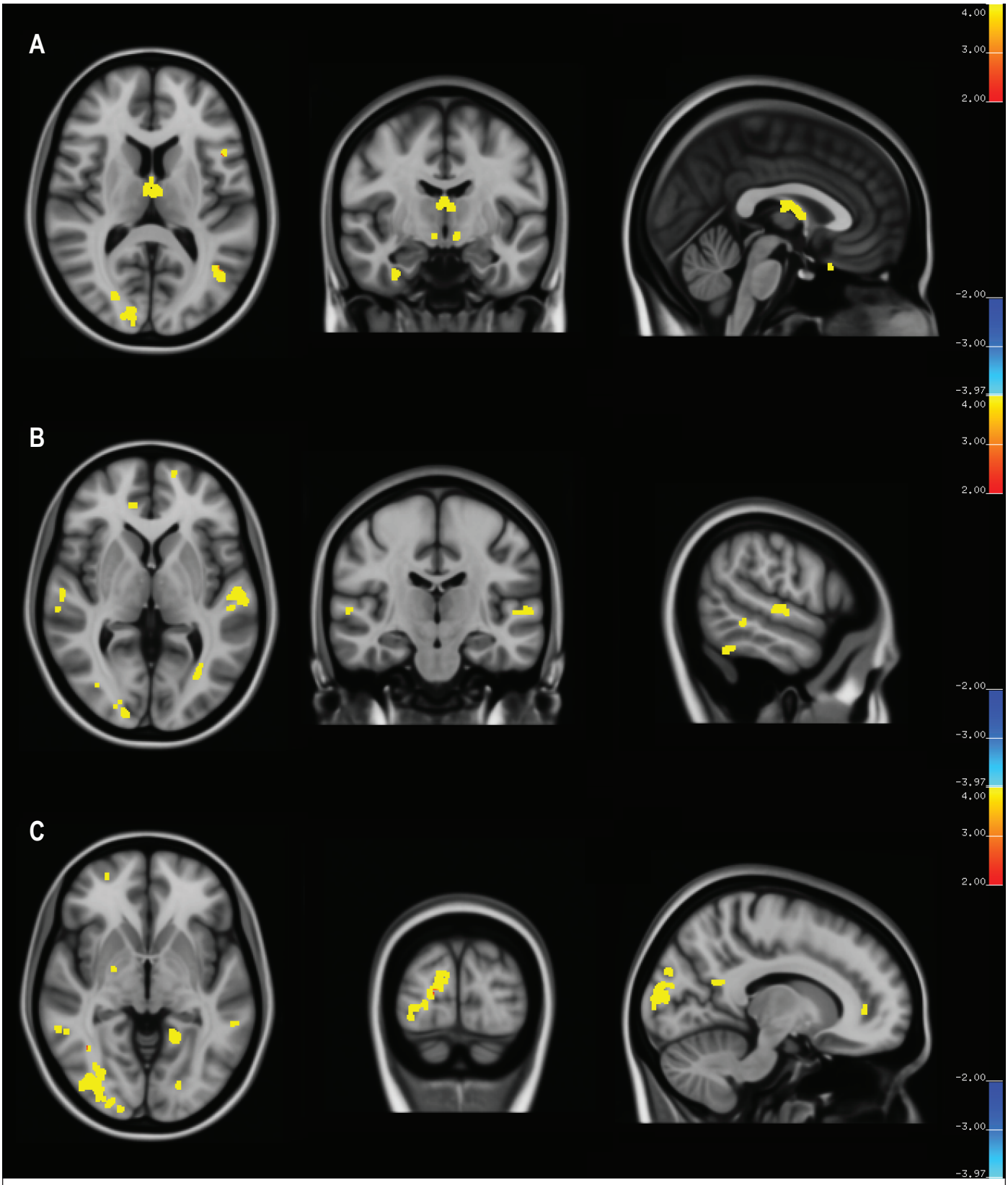

Figure S3—Regions with significant changes in radial diffusivity, a potential measure of myelin damage. Significant changes are displayed as the negative decadic logarithm of the P value ($P = 10^{-x}$). Panel A, fornix; panel B, left temporal cortex; panel C, right visual cortex. Increases in radial diffusivity are shown in red-yellow.

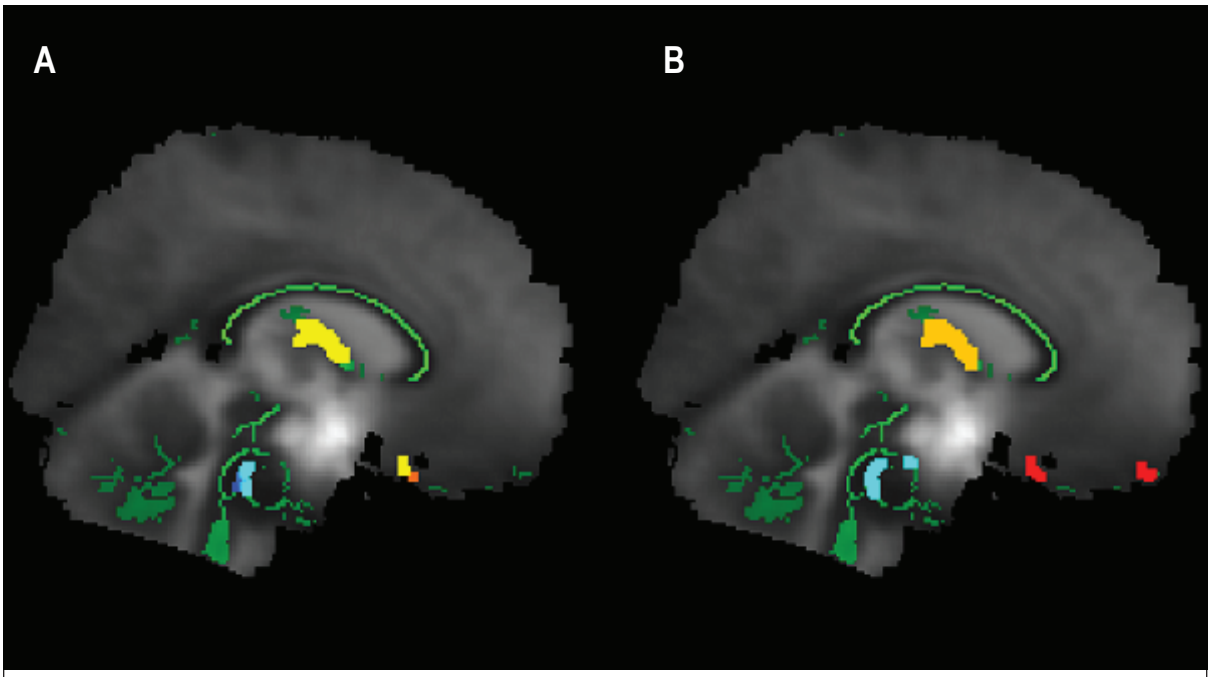

Figure S4—Sagittal view of the average b0 image and the overlaid white-matter skeleton (in green) showing the changes in radial diffusivity (red-yellow) and axial diffusivity (blue-light blue) using the randomize tools from Freesurfer package (A) and the FSL stream (B), as described in the methods section.

Annotations:

RBD	REM sleep behaviour disorder
MMSE	Mini Mental State Examination
NA	not applicable
TDI	threshold-discrimination-identification in Sniffin' Stick Test (a TDI sum score ≥ 30 is defined as normosmia) (Kobal et al., 2000)
FP-CIT	123I-N-Ω-fluoropropyl-2β-carbomethoxy-3β-(4-iodophenyl)-nortropane
SPECT	single photon emission computed tomography